Check for updates

ADVANCED MATERIALS TECHNOLOGIES
www.advmattechnol.de

Spectral Analysis on Color Detection Sharpness of Animal Vision toward Polychromatic Vision System

*Suyeon Lee, Hyochul Kim, Goohwan Kim, Hyungbin Son, and Un Jeong Kim**

Spectral discrimination by animal visions such as human, bird, and butterfly is numerically compared by angular analysis of photo-response (*PR*) which will be recorded at photo-receptors. Hyperspectral imaging system is utilized to simulate various animal vision. Bird vision is acute to discriminate colors among different vegetables due to its evenly spaced and narrow spectral responsivity of photo-receptors compared to that of human. Butterfly vision is excellent in discriminating red tomato ripening due to the exclusive photo-receptors detecting only over 600 nm. Even real and fake fruits in the same perceived color for human is discriminated by bird vision. Artificial vision with finely resolved polychromatic artificial cone cells are demonstrated surpassing human vision using visible multispectral camera. This provides insights on designing novel bio-inspired vision system.

1. Introduction

Vision system of living organisms is essential to obtain the information of their surroundings for their surviving such as finding predators, mates, preys, and etc. Common structure of eyes consists of lens and retina. Lens focuses incoming light onto retina which contains photo-receptors composed of cone and rod cells converting light into electrical signal, which is the initial step prior to perceiving color in brain through complicated neural processing. Cone cells among photo-receptors contain opsins which is photo sensitive proteins in the specific wavelength range, i.e., spectral response, and detect the corresponding wavelength range of the spectrum from the object. Its number, central wavelength and spectral width can vary depending on the animal species, and the structure and function of eyes has been diversified during their evolutional history.[1] Furthermore, the obtained image of each animal's vision is related not only to the opsins of photoreceptors but is also intricately connected to the structure of the lens, the density of photoreceptors, and the structure of the foveal pit.[2] For instance, the deep foveal pit in raptor eyes aids in magnification, allowing clearer object recognition.[3] Cephalopods like cuttlefish use polarization filters to enhance image contrast.[4]

Cameras have been developed as electronic devices functioning like a human eye capturing RGB images, and are currently prevalent in our daily and scientific life. There have been many efforts to adapt vision systems in nature by scientists who are interested in inventing novel types of camera.[5] Fisheye lens has been already commercialized for wide field of view (FOV), and compound eye mimicking cameras featuring distortion-free, wide FOV, and sensitive motion tracking imaging have been reported in the literatures.[5c–f] Among structural components of eye, artificial retina corresponding to RGB image sensors in digital camera must be the most important component when considering developing an innovative camera. There have been some efforts to develop novel artificial retina using optoelectronic memory devices,[6] photodiodes,[7] and phototransistors.[8] Even artificial cone cells are formed on the curved surface by soft electronics incorporating low dimensional materials.[8b] Besides, multispectral image sensors can be one of the best candidates possessing designable photo sensitive channels (CHs) as counterpart of RGB in its number and spectral width, which detects morphological images and the spectrum of the objects simultaneously. This technique is well established in the complementary metal oxide semiconductor (CMOS) compatible technology, and can be suitable to realize polychromatic vision system.[9]

Introducing various animal vision may be useful for novel camera development by emulating the behavior of insects and bird toward their living in selectivity and sensitivity manner. For example, bees and butterflies can see the way in petal to find honey with cone cell in UV range. Some birds can distinguish male and female with their feathers which look identical for human vision.[10] In recent work, the cancer imaging with UV spectral signature was successfully demonstrated using bio-inspired CMOS image senor including perovskite nanocrystals.[7b] In

S. Lee, H. Kim
Samsung Advanced Institute of Technology
Suwon, Gyeonggi 16678, Republic of Korea
G. Kim, H. Son
School of Integrative Engineering
Chung-Ang University
Seoul 06974, Republic of Korea
U. J. Kim
Department of physics
Dongguk University
Seoul 04620, Republic of Korea
E-mail: ujjanekim@dongguk.edu

The ORCID identification number(s) for the author(s) of this article can be found under https://doi.org/10.1002/admt.202400671

© 2024 The Author(s). Advanced Materials Technologies published by Wiley-VCH GmbH. This is an open access article under the terms of the Creative Commons Attribution License, which permits use, distribution and reproduction in any medium, provided the original work is properly cited.

DOI: 10.1002/admt.202400671

the literatures, animal UV and color visions have been simply compared on the same object along with human color vision. However, there is no scientific trials to investigate the detection acuity of color, the reflected light of the object under interest in the visible range, by incorporating the animal vision into spectroscopy. Using spectroscopy, it has been reported that color of vegetables, spectrum in the visible range, has been attributed to absorbance of anti-oxidants such as anthocyanin, β-carotene, lycopene, flavonoids, and chlorophyll.[11] Even the degree of ripeness of apples have been investigated based on the reflectance spectrum of lycopene and chlorophyll.[11a,f] Furthermore, prior to developing new types of artificial retina for high-performance novel camera, understanding spectral response at the cone cells of animal vision needs to be preceded.

In this work, various animal's visions have been successfully simulated using hyperspectral imaging system which offers high spectral resolution information based on conventional grating. Photo-response at cone cells for animal vision was successfully constructed for the visible spectrum of the same vegetables. From spectral response of cone cells, spectral discrimination capability of animal's vision system was numerically analyzed for bird as one of other branch of vertebrates, butterfly as a representative of invertebrates and human as a reference. Bird and butterfly vision are chosen to understand the color detection sharpness for various colored fruits and ripening of tomatoes as an example. Even though characteristics of images are intricately connected to the structure of vision system mentioned above, photo-response of cone cells by opsin is only considered in this work to investigate effect of spectral response of the vision system. Cone cells of two species are advantageous in distinguishing color even in the visible range compared to those of human. Even more butterfly's cone cells are found to be excellent in differentiating the degree of tomato ripening. In conjunction with Raman spectroscopy, relative concentration of lycopene might be obtained by photo-response of cone cells. Interestingly, bird vision is more powerful to distinguish real and fake vegetables with the same perceived color to human. Artificial eye vision with finely resolved polychromatic artificial cone cells was demonstrated surpassing human vision using snapshot type multispectral camera working in the visible range.

2. Result

2.1. Animal Vision and Artificial Eye Vision

Vision is the most dominant pathway to obtain information for human, known that humans depend on more than 70% of information on vision among five senses. However, vision system of human may not be the optimal structure among that of diverse animals. During the evolution, bird's ancestor had left four kinds of cone cells to their descendants (tetra-chromatic), including one cone cell sensitive even in ultraviolet range.[1a–c] On the other side, ancient mammals lost two kinds of cone cells out of four due to nocturnal behavior, and later some kind of mammals including primates and human became diurnal which had driven to gain third cone cell by genetic mutation and duplication (trichromatic). As a result, human's cone cells are not evenly spaced in wavelength which is attributed to genetic mutation and duplication unlike those of bird. Invertebrate including bees, butterflies, reptiles, shrimp and etc. have developed their own vision system with abundant kinds of sensitivity to wavelength of light from UV to IR.[1d–f,5a]

Figure 1 exhibits the normalized photo-sensitivity of cone cells of human, bird, and butterfly.[1a,d] For bird's cone cells, responsivity is relatively evenly spaced in wavelength and narrow in spectral width compared to those of human. For human and bird, three cone cells working in the visible range respond best to the light of short (S), medium (M), and long (L) wavelength. For human, responsivity is centered at 440 nm (S), 540 nm (M), and 570 nm (L) with 56 nm, 85 nm, and 110 nm of FWHM. As for bird, in particular budgerigar, its responsivity of cone cells is centered at 360 nm, 460 nm (S), 510 nm (M), and 570 nm (L) with 56 nm with 49 nm, 62 nm, and 60 nm of FWHM, respectively. About butterfly, there exists more diversity in responsivity of cone cells among species than bird, and furthermore, responsivity of one specific cone cell is differed by male or female as indicated in Figure 1. Responsivity of pieris rapae's is shown as a representative of butterfly's cone cells, centered at 360, 420 (for female), 440, 460 (for male), 580a, 580b, 620, and 640 nm with 56, 83, 89, 49, 104, 104, 51, and 40 nm of FWHM, respectively. Color of the object is strongly related to its spectrum in the visible range, i.e., reflected light from its surface. The perceived color for human is the final step in brain after complicated neural process of the photo-response values detected at each cone cell. The perceived color for non-human animals is difficult to know, but the photo-response for the given color, spectrum in the visible range, detected by its cone cells can be estimated. Depending on the animal vision, photo-response values can be differed for the same-colored object as represented in Figure 1. Simulation of particular animal vision was accomplished using grating-based line-scan type hyperspectral imaging system with high spectral and spatial resolution. Multispectral camera of which 16 CHs mimic cone cells working in the visible range can be developed to conduct artificial polychromatic vision to gather useful information outperforming human vision. The experimental details and set-up can be found in Experimental Section and Figure S1 (Supporting Information). Quantitative information from each type of photoreceptor depending on the animal vision will be discussed in this paper. Perception on color of object related to elaborate neural processing of the photo-response values is beyond the scope of this work.

2.2. Spectral Analysis on Bird Vision: Higher Acuity on Discerning Color

Figure 2 exhibits reflectance of various colored cherry tomatoes and blueberry obtained by line-scan type hyperspectral imaging system (details are in Methods) under halogen illumination as light source, and numerical analysis of photo-response observed by human and bird vision. Figure 2a,b is RGB images of samples taken by digital camera under white LED illumination and representative reflectance spectrum of each fruit under incident light of halogen lamp, respectively. Photo-response (PR) of each cone cell is determined as $\int R(\lambda)I(\lambda)\,d\lambda$ where $R(\lambda)$ is responsivity of cone cell, and $I(\lambda)$ is input spectrum, product of the incident light and reflectance of the object. For example, photo-response for L cone cell of human can be obtained by $h_L = \int R_L^h(\lambda)I(\lambda)\,d\lambda$ where

© 2024 The Author(s). Advanced Materials Technologies published by Wiley-VCH GmbH

2365709x, 2025, 3, Downloaded from https://advanced.onlinelibrary.wiley.com/doi/10.1002/admt.202400671 by Chung-Ang University, Wiley Online Library on [13/05/2026]. See the Terms and Conditions (https://onlinelibrary.wiley.com/terms-and-conditions) on Wiley Online Library for rules of use; OA articles are governed by the applicable Creative Commons License

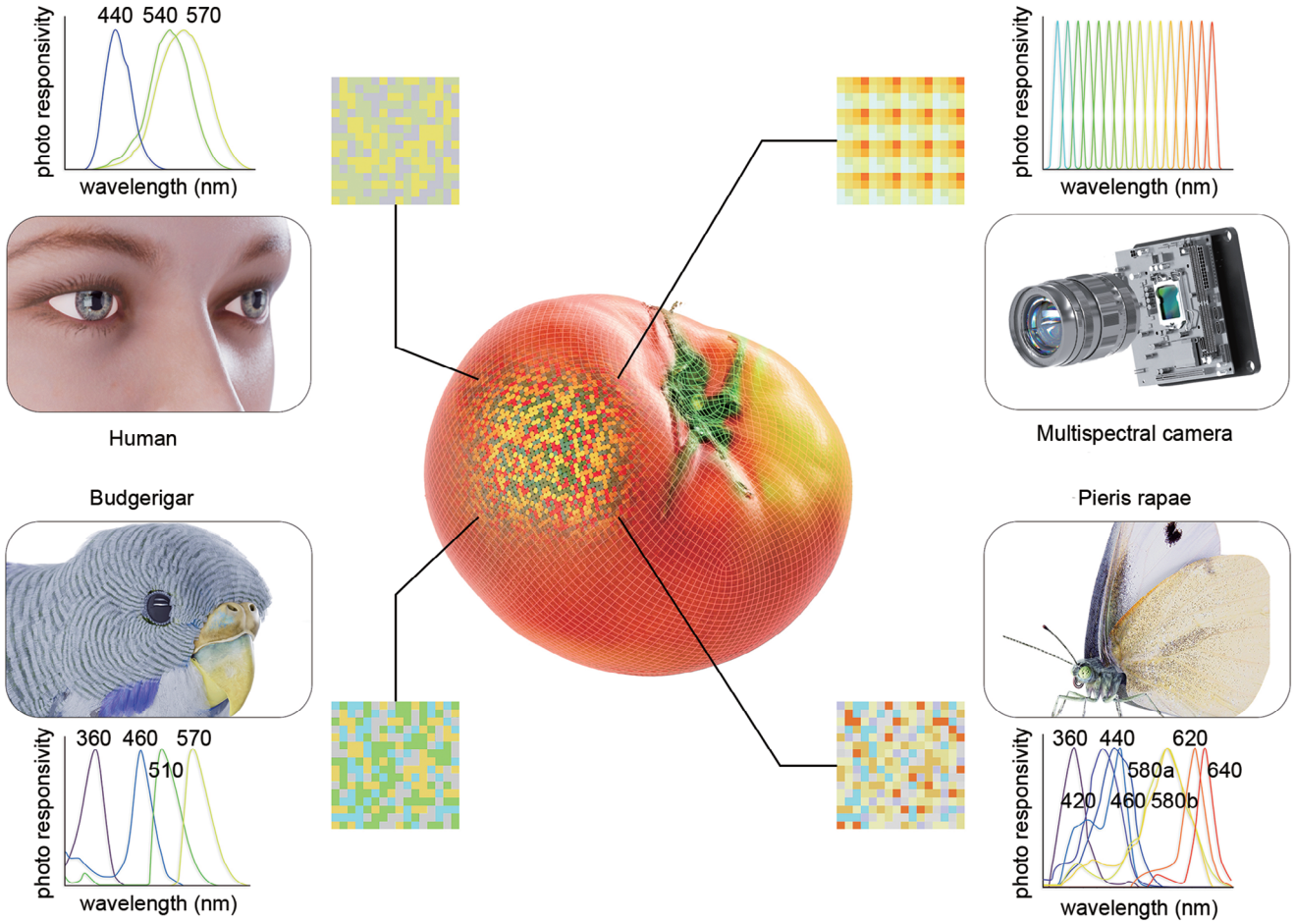


Figure 1. Photo-response of cone cells of human, budgerigar, and Pieris rapae is displayed, and the detected photo-response image at the cone cell for the same object. Snapshot type multispectral camera with 16 channels as artificial cone cells for the polychromatic artificial vision.

$R_L^h(\lambda)$ is response function of L cone cell of human. In nature, sensitivity of cone cell is depending on the wavelength, for example maximum sensitivity around 550 nm for human. Instead of using absolute responsivity, the normalized responsivity has been utilized not to give weight to specific wavelength for understanding its photo-response of animal vision effectively. Here, we denote detected photo-response value at human's and bird's cone cells as $\mathbf{h} = (h_L, h_M, h_S)$ and $\mathbf{b} = (b_L, b_M, b_S)$ where L, M, S represents cone cells for long, medium and short wavelength, respectively. Bird's UV sensitive cone cell is excluded because light source does not cover UV range. **h** and **b** for input spectrums in Figure 2b are shown in Figure 2c,d of which magnitude is normalized to 1, and **b** for various colored vegetables is well separated compared to **h**. This infers that bird vision can discriminate color of vegetables, in other word the reflected visible spectrum from them, with the amplified scale compared to human vision. The 3D vector, **h** and **b**, can be expressed in spherical coordinates as shown in Figure 2e,f, $\mathbf{h}=(h_r, h_\theta, h_\varphi)$ and $\mathbf{b}=(b_r, b_\theta, b_\varphi)$ for human and bird vision, respectively. r is radial distance (total intensity at cone cells), $\sqrt{h_L^2 + h_M^2 + h_S^2}$ and $\sqrt{b_L^2 + b_M^2 + b_S^2}$, θ is polar angle, $\arccos(h_S/h_r)$, and $\arccos(b_s/b_r)$, and φ is azimuthal angle, $\arccos\left(h_L/\sqrt{h_L^2 + h_M^2}\right)$ and $\arccos\left(b_L/\sqrt{b_L^2 + b_M^2}\right)$ for human and bird, respectively. Allowed range for $h_\theta(b_\theta)$ and $h_\varphi(b_\varphi)$ is from 0 to $\pi/2\pi$ because h_L, h_M and $h_S(b_L, b_M$ and $b_S)$ cannot be negative value. h_r exhibits 1.28 times larger value compared to b_r under halogen illumination in average due to wider FWHM of photo-responsivity of cone cells as shown in Figure 1. However, θ and φ component of bird's cone cells exhibits a larger angle variation among different colored vegetables compared to human's cone cells. Thus, bird vision has advantage in differentiating color among vegetables with higher acuity due to evenly spaced and sharper responsivity than human vision as shown in Figure 1 if intensity of illuminant is sufficient. Figure 2g,i,h,j is 2D map of angular component, $h_\theta(b_\theta)$ and $h_\varphi(b_\varphi)$, reconstructed from photo-response of cone cells. It is worth to mention that the distribution of θ component is crowded closer to $\pi/2$ due to relatively low reflectance under 500 nm in vegetables. When the reflectance is corrected by spectrum of halogen lamp, the color discrimination becomes prominently enhanced shown in Figure S2 (Supporting Information). It is worth to mention that photo-response is dependent on the illuminant condition, enhanced identifiability with illuminant correction, i.e., CIE illuminant E. The extracted photo-response values of each vegetable for Figure 2c–f and Figure S2b–e (Supporting Information) are the averaged value of 10 × 10 pixels after Gaussian denoising process spectrally and

© 2024 The Author(s). Advanced Materials Technologies published by Wiley-VCH GmbH

2365709x, 2025, 3, Downloaded from https://advanced.onlinelibrary.wiley.com/doi/10.1002/admt.202400671 by Chung-Ang University, Wiley Online Library on [13/05/2026]. See the Terms and Conditions (https://onlinelibrary.wiley.com/terms-and-conditions) on Wiley Online Library for rules of use; OA articles are governed by the applicable Creative Commons License

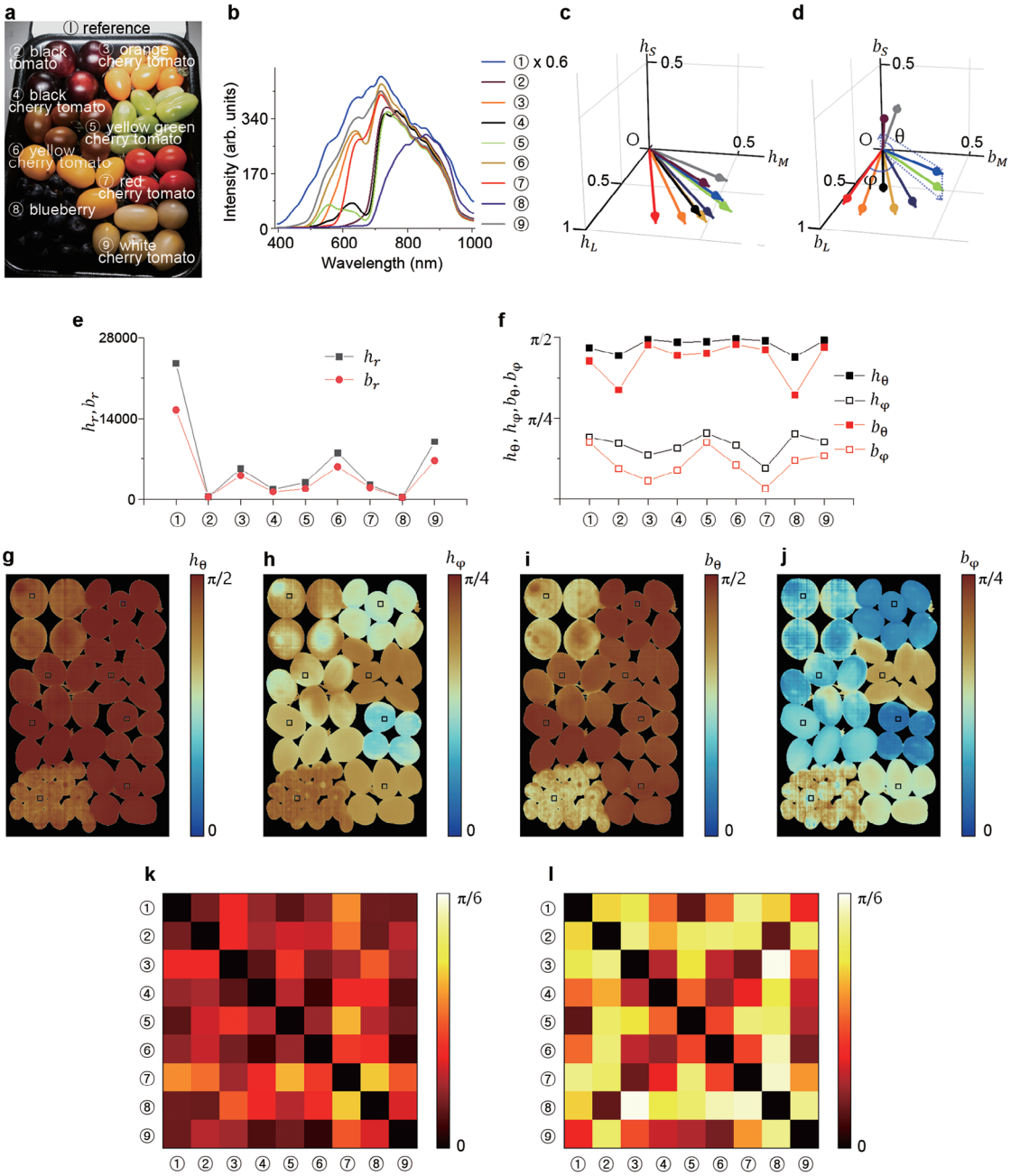


Figure 2. Color differentiation ability using angular analysis for human and bird vision. a) RGB image of cherry tomatoes with various colors and blueberries placed on the black tray. b) The reflectance spectrum of white reference bar and each vegetable under illumination of halogen lamp. Cross-polarization configuration for reflectance measurement was used to reduce speckles at the surface. Vector representation of the intensity at three photoreceptors c) (h_L, h_M, h_S) and d) (b_L, b_M, b_S) for human vision and bird vision in Cartesian coordinate system, respectively. Photo-response for various colored vegetable of human and bird into spherical coordinate system. e) Radial component at the photo-receptors of human (h_r) and bird (b_r) before normalization process against halogen lamp. f) The polar and azimuthal angle for human (h_θ, h_φ) and bird vision (b_θ, b_φ). 2D map of angular component (θ, φ) in spherical coordinate system for g, h) human and i, j) bird vision, respectively. Comparison matrix of angle (α) between various vegetables. The angle, α, between calculated photo-response at the trichromatic photoreceptor among other vegetable including the reference (white bar) for k) human and l) bird vision under halogen lamp.

spatially in hyperspectral images, indicated by the small open square in Figure 2g–j and Figure S2f–i (Supporting Information). The perceived color of vegetable can be more discernible by cone cells of bird than human because it can be defined by the difference or ratio among photo-response of cone cells depending on various kinds of color appearance model, not just by the intensity at each cone cell.[12]

This can be more intuitively understood in Figure 2k,l of which shows the comparison matrix representing the angle of **h** and **b** among other vegetables including the reference white plate,

© 2024 The Author(s). Advanced Materials Technologies published by Wiley-VCH GmbH

2365709x, 2025, 3, Downloaded from https://advanced.onlinelibrary.wiley.com/doi/10.1002/admt.202400671 by Chung-Ang University, Wiley Online Library on [13/05/2026]. See the Terms and Conditions (https://onlinelibrary.wiley.com/terms-and-conditions) on Wiley Online Library for rules of use; OA articles are governed by the applicable Creative Commons License

where angle, $\alpha = ((\mathbf{h}(i) \cdot \mathbf{h}(j))/(|\mathbf{h}(i)||\mathbf{h}(j)|))$, $i,j = ①,...⑨$. Comparison matrix clearly shows that photo-responsivity by bird vision enables to discriminate color by the reflected light from different vegetables with amplified acuity. Compared to human's cone cells, angle (α) by bird exhibits 1.4 greater value under halogen light. This result is originated from less overlapped photo-responsivity, evaluated numerically as cosine similarity, $\int a(\lambda)b(\lambda)d\lambda/(\sqrt{\int a^2(\lambda)d\lambda}\sqrt{\int b^2(\lambda)d\lambda})$ where $a(\lambda)$ and $b(\lambda)$ are spectrum under interest.[11f] Spectrums with cosine similarity value 1 are identical, and 0 means two spectra are orthogonal without overlap. L and M cone cells represent cosine similarity value 0.91 and 0.22 for human and bird, respectively. With incident light correction, angle (α) by bird was 1.9 times greater than human's cone cell as shown in Figure S2j,k (Supporting Information). As illuminant spectrum is corrected, photo-responsivities of cone cells get relatively equivalent rather than under halogen lamp both in human and bird vision, which result in higher value of angle (α). Even though α can show higher value for human than bird in specific cases, for example input spectrum has signal only over 500 nm resulting b_L dominant $\mathbf{b}$, the object ③ and ⑦, overall, bird vision shows higher value than human vision considering input spectrum in visible range.

In the literatures, color of plants has been known that it is mainly determined by content of antioxidants such as chlorophyll, anthocyanin, carotenoids (including β-carotene and lycopene), flavonoids and etc.[13] The kinds of antioxidant and its concentration for the selected samples were quantitatively measured by colorimetric analysis,[14] summarized in Table S1 (Supporting Information). As reported in the literature that relative concentration, and variety of flavonoids and carotenoids in vegetables have been discriminated by Raman spectroscopy,[11c,d] the kind of antioxidant in vegetables used for this study was further investigated by Raman spectroscopy with 532 nm excitation as shown in Figure S3 (Supporting Information). Three Raman bands at around 1010, 1160, and 1520 cm^{-1} have been assigned to C—CH_3 stretching mode (ν(C—CH_3)), C—C stretching mode (ν(C—C)) and C═C stretching mode (ν(C═C)) of carotenoids including lycopene, respectively.[11d] 1160 cm^{-1} and high frequency modes above 1550 cm^{-1} are associated with flavonoids as indicated in Figure S4 (Supporting Information).[11d] Yellow and white cherry tomatoes exhibit very low concentration of total carotenoid compared to the rest of cherry tomatoes as shown in Table S1 (Supporting Information). This is consistent with the results by Raman spectrum analysis as shown in Figure S3 (Supporting Information) where no noticeable signals from carotenoids were observed along with green tomato. Blueberry exhibits relatively high concentration of total anthocyanin (65.5 mg k^{-1}g) which was observed by Raman spectroscopy at 657 cm^{-1} and 725 cm^{-1}.

2.3. Detection of Post Maturity of Tomato by Butterfly Vision

Tomatoes turn its color during ripening from greenish to reddish, which is originated from degradation of chlorophyll followed by accumulation of carotenoid and flavonoid. Even more, there exist subtler color changes in postharvest ripening. There have been many efforts to determine the ripeness of tomatoes by Raman spectroscopy.[11d] In Figure S4a (Supporting Information), Raman spectrum of tomatoes was monitored as a function of storage time with 785 nm excitation. There are three distinctive Raman peaks around 1007, 1160, and 1520 cm^{-1} of carotenoids including lycopene, respectively. The intensity of three Raman peaks was linearly increased with adjusted R-square value of 0.4, 0.93, and 0.98 as shown in Figure S4b (Supporting Information). Even though Raman spectroscopy shows increase of lycopene concentration with post-maturity, this technique is limited for wide-field imaging to monitor the spatial distribution of its temporal changes.

The RGB images taken by digital camera and hyperspectral images from reflectance of tomatoes were monitored as a function of storage time at room temperature as shown in **Figure 3**. RGB images exhibit very barely distinguishable changes in colors with close observation as shown in Figure 3a. To quantify the color discrimination ability by RGB images, they are converted to CIELAB color space shown in Figure 3b. L, a^* and b^* are related to lightness (0 for black and 100 for white), green–red (negative value toward green, positive value toward red), blue–yellow (negative value toward blue, positive value toward yellow), respectively. The value a^* (b^*) was increased (decreased) and saturated after 5th day of storage, which means that the color of tomatoes become more reddish (less bluish) until 5th day due to ripening. Color difference in CIELAB color space can be represented by the Equation (1).

$$\Delta E^*_{ab} = \sqrt{\Delta L^2 + (\Delta a^*)^2 + (\Delta b^*)^2} \quad (1)$$

In Figure 3c, ΔE^*_{ab} between adjacent storage day are shown, and the case with ΔL exclusion is also shown as red dot with red line because it is related not to color but to brightness. The value for just-noticeable perceived color difference, $\Delta E^*_{ab,just}$ is found to be about 2.3[15] which means that the color change of tomato is not further noticeable for human after two days as shown as shaded area in Figure 3c.

The reflectance spectrum of tomato as a function of storage time up to 9th day is shown in Figure S5 (Supporting Information). The dip around 670 nm is originated from the absorption by chlorophyll b as shown in Figure S4c (Supporting Information), and gradually disappears with longer storage. Absorbance spectrum of monomer lycopene, i.e., the origin of tomatoes' red color, is shown in Figure S4c (Supporting Information).[11e] The broad peak around 550 nm is lowered and shifted to longer wavelength associated with J aggregation of lycopene with increasing its concentration with longer storage time. This seems to be J aggregation of monomer lycopene shown in Figure S4c (Supporting Information). J aggregation explains the reflectance edge around 600 *nm*.[11e] This corroborates that the experimental observation is related to decomposition of chlorophyll and increase of lycopene.[11d] The Raman intensity of lycopene increases linearly, but absorption by lycopene seems to saturate with the longer storage time, respectively.

We investigate how cone cells of human and bird response to spectral change of tomato during post-maturity. Intensity value at each cone cell for human, (h_L, h_M, h_S) and bird, (b_L, b_M, b_S) are calculated as shown in Figure 3d,f where the spectrum is

© 2024 The Author(s). Advanced Materials Technologies published by Wiley-VCH GmbH

2365709x, 2025, 3, Downloaded from https://advanced.onlinelibrary.wiley.com/doi/10.1002/admt.202400671 by Chung-Ang University, Wiley Online Library on [13/05/2026]. See the Terms and Conditions (https://onlinelibrary.wiley.com/terms-and-conditions) on Wiley Online Library for rules of use; OA articles are governed by the applicable Creative Commons License

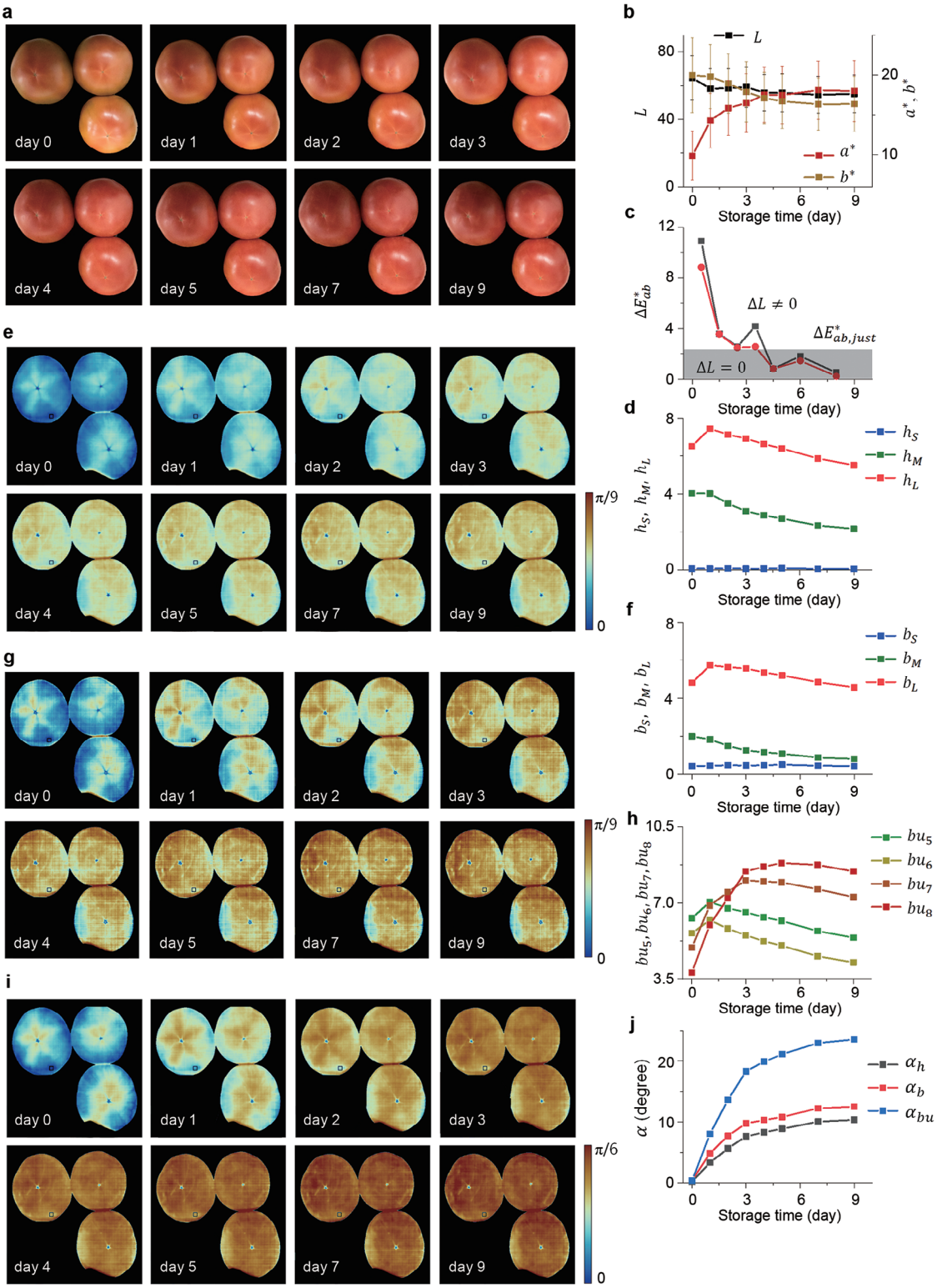


Figure 3. Post-maturity measured by human and butterfly vision. a) RGB images of red tomatoes as a function of storage time. b) ***L***, *a** and *b** values as a function of storage time extracted from RGB images converting to CIELAB color space. c) Color difference in CIELAB color space, E^*_{ab}, with and without consideration of ΔL, d) the intensity at three photoreceptors (h_L, h_M, h_S) for human vision, e) 2D map of angular shift against reference point at 0th storage time for human vision, f) (b_L, b_M, b_S) values as a function of storage time, and g) 2D image of angle (α) against 0th day. h) The intensity at four photoreceptors (bu_5, bu_6, bu_7, bu_8) for butterfly vision, i) 2D map of angular shift against reference point at 0th storage time for butterfly vision, j) the angle (α) calculated against the reference point indicated by the square in the image at 0th day during post-maturity.

© 2024 The Author(s). Advanced Materials Technologies published by Wiley-VCH GmbH

2365709x, 2025, 3, Downloaded from https://advanced.onlinelibrary.wiley.com/doi/10.1002/admt.202400671 by Chung-Ang University, Wiley Online Library on [13/05/2026]. See the Terms and Conditions (https://onlinelibrary.wiley.com/terms-and-conditions) on Wiley Online Library for rules of use; OA articles are governed by the applicable Creative Commons License

normalized by the illuminant. The value of (h_L, h_M, h_S) and (b_L, b_M, b_S) is gradually decreased after 1st day of storage time while h_S and b_S remained negligible or zero because of nearly zero reflectance below 500 nm as shown Figure S5 (Supporting Information). To quantify response change with tomato ripening both for human and bird, angular analysis against reference photo-response indicated by small square at 0th day allows to monitor photo-response distribution within the samples and its changes with longer storage time. Figure 3e,g exhibits angular change of photo-response against 0th day by human and bird vision as a function of storage time. α_h and α_b changes up to 10.4 and 12.5 degree until 9th day for human and bird vision in Figure 3j. Threshold angular shift for just-noticeable perceived color difference, α_{just}, can be defined by about 2 degree deduced from $\Delta E^*_{ab,\,just} \approx 2.3$. We investigate butterfly vision which possesses more various photo-receptors than vertebrates as shown in Figure 1. For ripening of tomatoes, among eight photo-receptors, four photo-receptors with shorter wavelength response will not participate in perceiving tomato ripening according to its reflectance spectrum. Response of the remaining four (580a, 580b, 620, 640 nm) cone cells of butterfly, which are related to reflectance spectrum of tomatoes, are denoted as $\mathbf{bu} = (bu_5, bu_6, bu_7, bu_8)$, respectively. The photo-response value of each cone cell component (bu_5, bu_6, bu_7, bu_8) is calculated as displayed in Figure 3h after correction of halogen illuminant. For butterfly, the response of two cone cells corresponding to 580 nm, bu_5 and bu_6, exhibit similar behavior to that for human, h_L and h_M. But the intensity of other two cone cells with longer wavelength response, bu_7 and bu_8, increase until 3rd or 5th day of storage time and saturate or slightly decrease as shown in Figure 3h. Due to distinct change of response, α_{bu} of photo-response for butterfly against reference indicated by open square on tomatoes exhibits larger changes than α_h and α_b in Figure 3i. As seen in Figure 3j, α_{bu} was increased up to 23.6 degree up to 9th day of storage which is two times larger than that for human. Angle between adjacent days of human, bird and butterfly vision decreases from 3.3, 4.8 and 8.1 degree between 0th and 1st day, respectively. Angle between 2nd and 3rd day for human and bird vision is at the boundary, α_{just} with the value 2.0 and 2.1, which means barely noticeable with human and bird vision. However, angle for butterfly vision is 4.7, still higher than α_{just}. This indicates that butterfly vision is more sensitive for detecting red tomato ripening. When we consider noticeable difference, $\alpha_{just} = 2$, corresponding value for $\Delta E^*_{ab,\,just} \approx 2.3$, human and bird hardly distinguish between 2nd and 3rd day, i.e., $\alpha \approx 2$, but butterfly can distinguish due to α= 4.7. Even after 4th day, α between adjacent days starts to saturate due to post-maturity, but butterfly vision maintained higher α than human and bird vision.

As conventional RGB camera is developed to function and record as human's eye, snapshot type multispectral camera can be considered as artificial eye with polychromatic artificial retina. Multispectral image sensor is advantageous to engineer the spectral range, responsivity (spectral width) and the number of CHs to realize the polychromatic artificial vision depending on the purposes. Periodic array of 16 CHs for polychromatic artificial vision is fabricated on the image sensor replacing RGB color filter on the image sensor. (See Methods) 16 distributed Bragg reflectors (DBRs) based filters are formed by plasma enhanced chemical vapor deposition (PECVD) and photolithography, and its resonant wavelength is adjusted by the thickness of the SiO_2 cavity layer. The detailed material and structure of DBR used in this work can be found in Figure S6 (Supporting Information) and fabrication process can be found in the previous work.[9,16] **Figure 4** exhibits snapshot type multispectral camera which has 16 CHs in the range of 490–628 nm with 5–10 nm FWHM. The spectral characteristics of each CH (transmission of filter × quantum efficiency (QE) of pixels in the image sensor) are shown in Figure 4a with photo-response curves of four photo receptors for butterfly vision. Compared to animal vision including butterfly, in snapshot type multispectral camera, much narrower FWHM of filters is advantageous to monitor subtle spectral change, but range of spectral response is limited instead. We monitored ripening of tomatoes with multispectral camera as a function of storage time and the normalized intensity by its total intensity is shown in Figure 4b. Angular shift for multispectral camera, α_{MSC} between 0th and 9th day is 14.8 degree as shown in Figure 4c. 2D angular shift images as a function of storage time are shown in Figure 4d. Black open squares denotes 10 × 10 pixels to calculate angular shift in Figure 4c. By designing the spectral characteristics of multispectral camera, color distinction ability can be largely enhanced.

As a circumstance in real life, three kinds of ripe tomatoes, purchased from different distribution channel and brand name at unknown ripeness stage, were investigated in terms of lycopene concentration from its color. Concentration of lycopene has been compared by Raman spectrum of three kinds of tomatoes as shown in Figure S7 (Supporting Information). $Tomato_2$ exhibits much lower Raman intensity by about two times at 0th day compared to $Tomato_1$ and $Tomato_3$. The intensity level of Raman spectrum of three kinds of tomatoes tends to be merged after 14 days. By continuous observation of those tomatoes, changes in color might be noticed from RGB images in **Figure 5**. For 14 days, $tomato_1$ and $tomato_3$ changed its color lower than $\Delta E^*_{ab,just} \approx 2.3$ but 11.9 for $tomato_2$ ignoring ΔL term. However, with 14 days storage, all tomatoes were fully ripened and ΔE^*_{ab} between three tomato groups are still largely scattered in the range of 1.2–5.1. ΔE^*_{ab} can be deduced from Figure 5b. Even though the value of ΔE^*_{ab} among tomato groups are slightly reduced from 4.3 to 8.3 of 0th day of purchase, it is hard to distinguish ripeness based on ΔE^*_{ab} among tomatoes. Scattered ΔE^*_{ab} among tomatoes would be affected by speckles and shadows on the samples. To understand the ripeness state of the purchased tomatoes, we choose the same reference point at 0th day in Figure 3d,h for human and butterfly vision, respectively. 2D image of α_h and α_{bu} was constructed against the reference points shown in Figure 5c,e. The average α_h and α_{bu} of 10 × 10 pixels for the reflected light indicated by black solid rectangle is shown in Figure 5d,f. Base on the analysis of Figure 3, $tomato_1$, $tomato_2$ and $tomato_3$ at 0th day exhibits the ripeness stage of 9th, 2nd and 7th day in human vision, and 9th, 2nd and 5th day in butterfly vision, respectively. All tomatoes at 14th day exhibits 9th day ripeness stage both in human and butterfly vision, as expressed in right side of graphs. Difference in α_h and α_{bu} of $tomato_2$ from 0th to 14th day was found to be 4.9 and 10.9 degree, respectively. Its angle for $tomato_2$ was found to be merged to the same value with $tomato_1$ and $tomato_3$ in Figure 3d,f. As shown in the figures, butterfly vision exhibits

© 2024 The Author(s). Advanced Materials Technologies published by Wiley-VCH GmbH

2365709x, 2025, 3, Downloaded from https://advanced.onlinelibrary.wiley.com/doi/10.1002/admt.202400671 by Chung-Ang University, Wiley Online Library on [13/05/2026]. See the Terms and Conditions (https://onlinelibrary.wiley.com/terms-and-conditions) on Wiley Online Library for rules of use; OA articles are governed by the applicable Creative Commons License

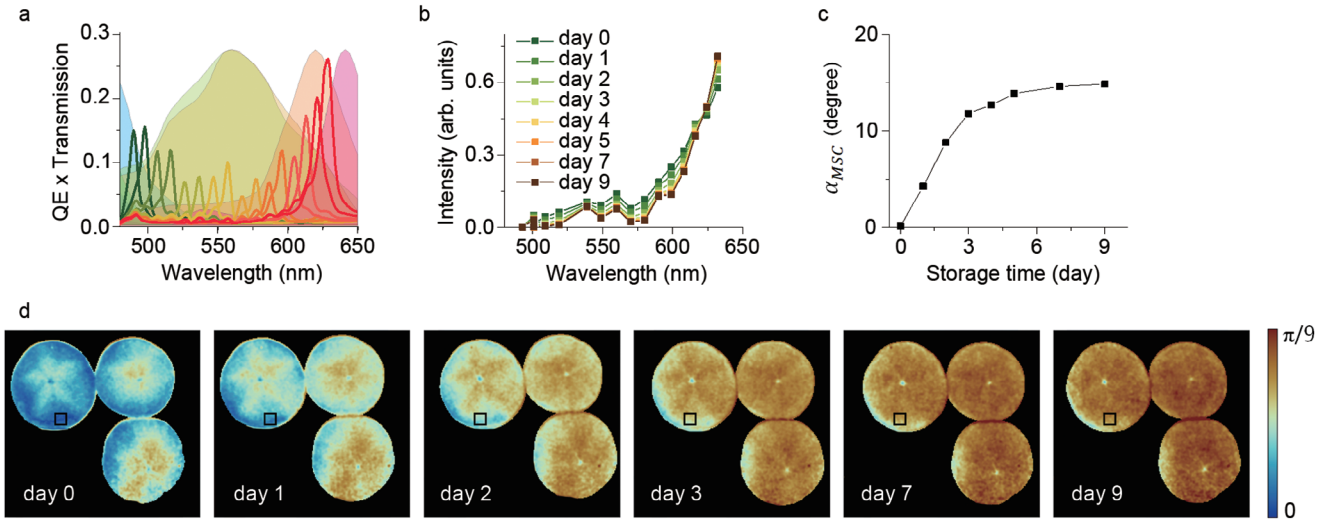


Figure 4. Artificial polychromatic vision by 16 CH multispectral camera. a) The transmission characteristics of each CH (transmission × quantum efficiency (QE)) of snapshot type multispectral camera overlaid with four photo-response curves for butterfly vision. b) Normalized intensity by total intensity accumulated at each CH from 16 CH as a function of storage time. c) α at each storage time against the angle at 0th storage day. d) 2D map of α with longer storage time against the reference point indicated by open square at 0th storage day.

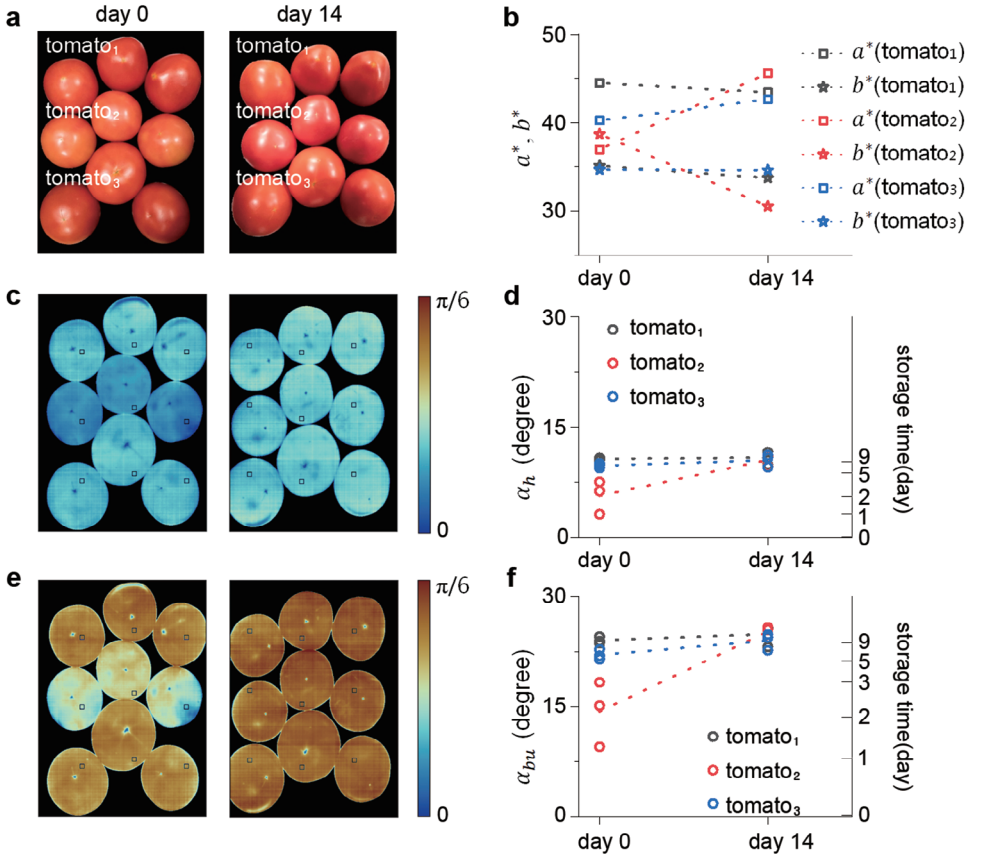


Figure 5. Detection of the unknown ripeness of tomatoes by butterfly vision. a) RGB image of three kinds of purchased tomatoes indicated by tomato$_1$, tomato$_2$ and tomato$_3$ at the unknown ripeness at 0th and 14th day of storage. b) a^* and b^* values of tomato$_1$, tomato$_2$ and tomato$_3$. c) the 2D image of angle, α_h and d) the representative angle, α_h, between the point indicated by open square against the reference at 0th day in Figure 3d to estimate the ripeness of the purchased tomatoes. e) the 2D image of angle, α_{bu} and f) the representative angle, α_{bu}, between the point indicated by open square against the reference at 0th day in Figure 3h.

© 2024 The Author(s). Advanced Materials Technologies published by Wiley-VCH GmbH

2365709x, 2025, 3, Downloaded from https://advanced.onlinelibrary.wiley.com/doi/10.1002/admt.202400671 by Chung-Ang University, Wiley Online Library on [13/05/2026]. See the Terms and Conditions (https://onlinelibrary.wiley.com/terms-and-conditions) on Wiley Online Library for rules of use; OA articles are governed by the applicable Creative Commons License

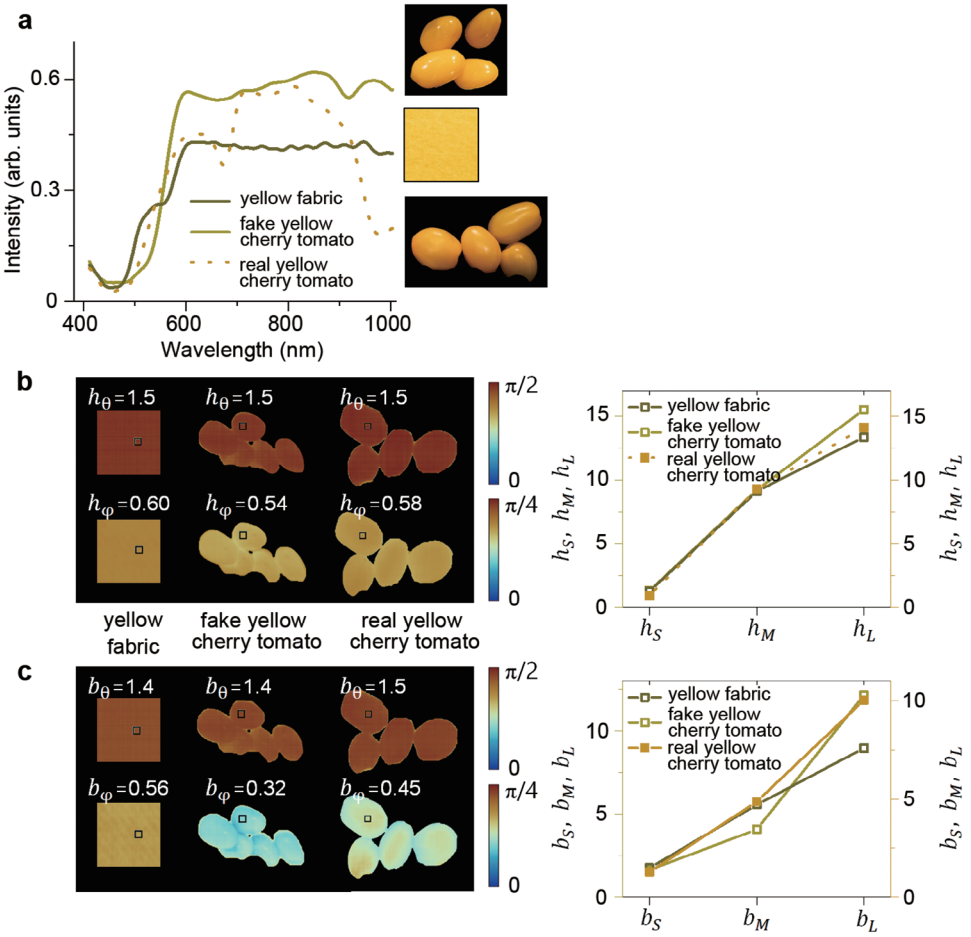


Figure 6. Discrimination of real and fake yellow cherry tomato by animal vision. a) The reflection spectrum of three yellow objects, fabric, fake, and real cherry tomatoes. Photo-response of three yellow objects in b) human and c) bird vision in the Cartesian coordinates and θ and φ components, and the averaged (h_L, h_M, h_S) and (b_L, b_M, b_S) values of 10 × 10 pixels indicated by open square in the image.

much enhanced α_{bu} among tomatoes at 0th and detects further ripening of tomatoes at 14th day. From this observation, concentration of lycopene could be qualitatively analyzed by α_{bu}.

2.4. Distinction of the Real from Imitations based on its Visible Spectrum

As another proof concept, objects with the same color to human can be differentiated by introducing non-human vision. There may exist countless number of input spectrum, $I_\lambda(\lambda)$ which produces the same photo response, PR, determined by $\int R(\lambda)I(\lambda)\,d\lambda$. Any intelligence algorithm cannot be applied to distinguish the items having the same value of PRs for a certain vision system. For example, various kinds of illuminants, LED, fluorescent light, sunlight, and etc. producing the different spectral characteristics cannot be distinguishable by human vision. As a demonstration, discriminating real and fake cherry tomatoes were tested using human and bird vision in **Figure 6**. The spectrum of yellow felt, fake and real cherry tomatoes are compared in Figure 6a which exhibits slight difference in the visible range. These are not distinguishable by RGB cameras and human vision. By human vision, the photo-response of the long wavelength photo-receptor exhibits slightly different value for three objects in Figure 6b. However, by bird vision, photo-response of medium and long photo-receptor varied significantly in Figure 6c. The images of θ and φ components converted from Cartesian coordinates are displayed in Figure 6b,c. The average values of θ and φ in 10 × 10 pixels are indicated in each image. Angle (α) between real yellow cherry tomato and yellow fabric was found to be 1.6, by human but 6.5 in bird vision, respectively. Angle between real and fake yellow cherry tomatoes is found to be 2.8 and 7.3 by human and bird vision, respectively. Enhancement effect can be dependent on the situation, for example, objects and illuminant condition. As a yellow green case, the same analysis has been done using yellow green cherry tomato and fake green grape, as shown in Figure S8 (Supporting Information). In that case, angle is enhanced from 3.3 to 4.7, relatively lower than yellow objects. This substantiates bird vision is proper to distinguish even real and fake items in yellow than yellow green color. From this analysis, by choosing proper animal vision, counterfeit items in the market can be sorted out from genuine items.

As observed in the experimental data, illumination is also important for the perception of color.[17] Under various illuminant

 © 2024 The Author(s). Advanced Materials Technologies published by Wiley-VCH GmbH

2365709x, 2025, 3, Downloaded from https://advanced.onlinelibrary.wiley.com/doi/10.1002/admt.202400671 by Chung-Ang University, Wiley Online Library on [13/05/2026]. See the Terms and Conditions (https://onlinelibrary.wiley.com/terms-and-conditions) on Wiley Online Library for rules of use; OA articles are governed by the applicable Creative Commons License

condition, response at the photo-receptors must be another subject to investigate for color detection sharpness. Also, perception could be differed if the reflected surface is textured (e.g., bifringence material), and its reflection property would be changed at different angles.[5f] Furthermore, depending on the eye structure such as single or compound eye, the effective incident angle to the eye may be differed so that its eye response to angular reflection.[5c–f] The effect of polarization of illuminant and effect of eye structure needs to be investigated in the future in terms of vision system of animal.

3. Conclusion

Here, color detection sharpness by various animal vision has been investigated on colored vegetables and red tomato's postmaturity as a test bed by numerical analysis of photo-response at the cone cells. This can be simulated using hyperspectral images of reflectance in the visible range from the objects, its color. By introducing animal vision, real and fake objects can be easily distinguishable which look identical to human due to its same photo-response. This work substantiates that animal's color vision can be sharper than human. 16 CH snapshot type multispectral camera with narrow responsivity has been demonstrated as artificial eye having polychromatic artificial cone cells outperforming human eye. By the hint on the animal vision, developing novel "bio-inspired" artificial eye can stimulate for the enhanced performance and new functions in camera. In the future, considering "perception", i.e., imaging processing in various neural activity and brain, proper image signal processing (ISP) algorithm will maximize the performance and diversity of artificial eye function. Also, trade-off between spatial resolution and number of channels due to the limitation of the number of pixels in the image sensor could be overcome by developing new types of image sensors, such as vertically stacked photodiodes.[7b,18] By designing dynamic range, spectral width, and its number of CH sets as polychromatic cone cells and proper algorithm, intriguing artificial eye vision can be devised prosperously for smartphone business and various sensor applications including smart farming, forgery prevention technology and etc.

4. Experimental Section

Sample Preparation: Fruits and vegetables were purchased from local markets in Suwon, South Korea.

Methods: Hyperspectral images of reflectance of samples were obtained in line-scan mode by FX10 from Specim, Inc. working in the 410–1000 nm region with 2.6–2.8 nm spectral resolution. Cross-polarization configuration was used to remove speckles which are directly reflected light from the sample surface. One polarizer (ultra-broadband wire grid polarizers, Thorlabs Inc.) at the halogen lamps and the other polarizer at the detector are aligned perpendicular to each other. Tray is mechanically moved to carry the objects for line scanning of reflectance data. 878 frames recorded with 10 Hz frame rate, 512 pixels, and 20 ms (for Figures 2, 5, and 6)/12 ms (for Figure 3) integration time.

RGB images of samples were obtain by Galaxy S21 from Samsung under illumination of white LED and halogen.

SM-N960U 1/100 s (Figure 2) 1/60 s (Figure 3)

Raman spectrum of samples was acquired using a Nanobase (XperRam 200) instrument equipped with 785 nm and 532 nm laser excitation with a special probe for excitation and collection. Raman signal was collected by contact mode on the surface of fruits so that ripening of tomatoes was monitored without cutting it.

Concentration of antioxidants (total anthocyanin, total flavonoid, total chlorophyll, total polyphenol, total carotenoids) in fruits and vegetables were quantified by colorimetric analysis.[14] Samples for colorimetric analysis were prepared only using flesh of fruits.

Fabrication of Snapshot type Multispectral Camera: A 16 band-pass filter arrays working in the range of 490–630 nm was fabricated on the Samsung's CMOS image sensor. Instead of conventional RGB filters, bandpass filters are fabricated, composed of a SiO_2 resonator sandwiched between top distributed Bragg reflector (DBR) and bottom DBR. Top DBR is 5 pairs of SiO_2/TiO_2, and bottom DBR is mirror imaged structure of the top DBR, fabricated with 10 steps of PECVD process. Thickness of SiO_2 and TiO_2 in DBR is determined by $\lambda_{peak}/4n$, where λ_{peak} and n are peak wavelength of the filter and refractive index of the material at the wavelength, respectively. Thickness of SiO_2 resonator was varied by 16 cases using 4 times binary photo/etching fabrication process. The size of pixel in image sensor is 1.4 μm and we use 2×2 pixels for each CH. The number of pixels in the image sensor is 2608×1960, thus each channel periodically arranged in mosaic pattern corresponds to 652×490 pixels. Images were taken with 100 ms integration time, 1 analogue gain and 1 digital gain by the multispectral camera.

Supporting Information

Supporting Information is available from the Wiley Online Library or from the author.

Acknowledgements

This work was supported by the Samsung Advanced Institute of Technology (SAIT) and by the Chung-Ang University Research Scholarship Grants in 2023.

Conflict of Interest

The authors declare no conflict of interest.

Author Contributions

S.L. and U.J.K. were responsible for conceptualization. Methodology was developed by U.J.K., S.L., G.K., and H.S. The investigation was carried out by U.J.K., S.L., G.K., and H.C.K. Visualization was managed by S.L. and U.J.K. H.S. acquired the funding. Supervision was provided by S.L. and U.J.K. The original draft was written by S.L. and U.J.K. Review and editing were performed by S.L., H.C.K., G.K., H.S., and U.J.K. All authors confirmed the final manuscript.

Data Availability Statement

The data that support the findings of this study are available from the corresponding author upon reasonable request.

Keywords

animal vision, artificial vision, hyperspectral camera, polychromatic vision system

Received: April 27, 2024
Revised: August 20, 2024
Published online: September 19, 2024

© 2024 The Author(s). Advanced Materials Technologies published by Wiley-VCH GmbH

2365709x, 2025, 3, Downloaded from https://advanced.onlinelibrary.wiley.com/doi/10.1002/admt.202400671 by Chung-Ang University, Wiley Online Library on [13/05/2026]. See the Terms and Conditions (https://onlinelibrary.wiley.com/terms-and-conditions) on Wiley Online Library for rules of use; OA articles are governed by the applicable Creative Commons License

[1] a) T. H. Goldsmith, *Vis. Neurosci.* **2013**, *30*, 21; b) J. Falcón, A. Torriglia, D. Attia, F. Viénot, C. Gronfier, F. Behar-Cohen, C. Martinsons, D. Hicks, *Front. Neurosci.* **2020**, *14*, 1183; c) T. H. Goldsmith, *Sci. Am.* **2006**, *295*, 68; d) J. Marshall, K. Arikawa, *Curr. Biol.* **2014**, *24*, R1150; e) E. Warrant, Cambridge University Press, **2006**; f) B.-M. Song, C.-H. Lee, *Front. Neural Circuits* **2018**, *12*, 16.
[2] A. Bringmann, *Anatomia, Histologia, Embryologia* **2019**, *48*, 177.
[3] a) B. Xu, Z. Li, B. Cheng, Y. Yang, A. Siddique, *Remote Sensing* **2023**, *15*, 2106.; b) A. W. Snyder, W. H. Miller, *Nature* **1978**, *275*, 127.
[4] N. Shashar, R. Hagan, J. G. Boal, R. T. Hanlon, *Vis. Res.* **2000**, *40*, 71.
[5] a) L. P. Lee, R. Szema, *Science* **2005**, *310*, 1148; b) L. Dong, A. K. Agarwal, D. J. Beebe, H. Jiang, *Nature* **2006**, *442*, 551; c) G. J. Lee, C. Choi, D. H. Kim, Y. M. Song, *Adv. Funct. Mater.* **2018**, *28*, 1705202; d) Y. M. Song, Y. Xie, V. Malyarchuk, J. Xiao, I. Jung, K.-J. Choi, Z. Liu, H. Park, C. Lu, R.-H. Kim, *Nature* **2013**, *497*, 95; e) K.-H. Jeong, J. Kim, L. P. Lee, *Science* **2006**, *312*, 557; f) M. Ryu, M. Han, L. Grineviciute, J. Hu, T. Moein, R. Honda, T. Katkus, M. J. Tobin, J. Vongsvivut, T. Tolenis, Y. Nishijima, S. H. Ng, S. Juodkazis, J. Morikawa, *Laser Photonics Rev.* **2023**, *17*, 2200535.
[6] a) Y. Cai, Y. Jiang, C. Sheng, Z. Wu, L. Chen, B. Tian, C. Duan, S. Xiong, Y. Zhan, C. Cong, *npj Flexible Electron.* **2023**, *7*, 29; b) F. Zhou, Z. Zhou, J. Chen, T. H. Choy, J. Wang, N. Zhang, Z. Lin, S. Yu, J. Kang, H. S. P. Wong, *Nat. Nanotechnol.* **2019**, *14*, 776; c) X. Fu, T. Li, B. Cai, J. Miao, G. N. Panin, X. Ma, J. Wang, X. Jiang, Q. Li, Y. Dong, *Light: Sci. Appl.* **2023**, *12*, 39.
[7] a) M. Kim, G. J. Lee, C. Choi, M. S. Kim, M. Lee, S. Liu, K. W. Cho, H. M. Kim, H. Cho, M. K. Choi, *Nat. Electron.* **2020**, *3*, 546; b) C. Chen, Z. Wang, J. Wu, Z. Deng, T. Zhang, Z. Zhu, Y. Jin, B. Lew, I. Srivastava, Z. Liang, *Sci. Adv.* **2023**, *9*, eadk3860.
[8] a) F. Liao, Z. Zhou, B. J. Kim, J. Chen, J. Wang, T. Wan, Y. Zhou, A. T. Hoang, C. Wang, J. Kang, *Nat. Electron.* **2022**, *5*, 84; b) C. Choi, M. K. Choi, S. Liu, M. Kim, O. K. Park, C. Im, J. Kim, X. Qin, G. J. Lee, K. W. Cho, *Nat. Commun.* **2017**, *8*, 1664.
[9] U. J. Kim, S. Lee, H. Kim, Y. Roh, S. Han, H. Kim, Y. Park, S. Kim, M. J. Chung, H. Son, *Nat. Commun.* **2023**, *14*, 5262.
[10] M. D. Eaton, *Proc. Natl. Acad. Sci. USA* **2005**, *102*, 10942.
[11] a) M. N. Merzlyak, A. E. Solovchenko, A. A. Gitelson, *Postharvest. Biol. Technol.* **2003**, *27*, 197; b) F. Nekvapil, I. Brezestean, D. Barchewitz, B. Glamuzina, V. Chiş, S. C. Pinzaru, *Food Chem.* **2018**, *242*, 560; c) H. Akpolat, M. Barineau, K. A. Jackson, M. Z. Akpolat, D. M. Francis, Y.-J. Chen, L. E. Rodriguez-Saona, *Sensors* **2020**, *20*, 3723; d) M. T. C. Campos, L. F. Maia, H. F. Dos Santos, H. G. M. Edwards, L. F. C. de Oliveira, *J. Raman Spectrosc.* **2023**, *54*, 1314; e) M. Ishigaki, P. Meksiarun, Y. Kitahama, L. Zhang, H. Hashimoto, T. Genkawa, Y. Ozaki, *J. Phys. Chem. B* **2017**, *121*, 8046; f) J. W. Park, J. Jeon, G. B. Kim, K. H. Jeong, *Adv. Sci.* **2023**, *10*, 2304320.
[12] M. D. Fairchild, in *Color Appearance Models*, John Wiley & Sons, New York **2013**.
[13] E. D. Cömert, B. A. Mogol, V. Gökmen, *Current Res. Food Sci.* **2020**, *2*, 1.
[14] Health Functional Food Code from Ministry of Food and Drug Safety. MFDS, Ed **2023**.
[15] S. Gaurav, B. Raja, in *Digital Color Imaging Handbook*, CRC Press, Boca Raton **2003**.
[16] Y. Park, U. J. Kim, S. Lee, H. Kim, J. Kim, H. Ma, H. Son, Y. Z. Yoon, J.-s. Lee, M. Park, H. Choo, Q. H. Park, Y.-G. Roh, *Sens. Actuators, B* **2023**, *381*, 133442.
[17] C. Weerasuriya, S. H. Ng, W. Woods, T. Johnstone, P. Vitta, L. Hugrass, S. Juodkazis, *Appl. Sci.* **2023**, *13*, 2988.
[18] A. Rush, P. Hubel, *J. Soc. Photograph. Sci. Technol. Japan* **2003**, *66*, 57.

© 2024 The Author(s). Advanced Materials Technologies published by Wiley-VCH GmbH

2365709x, 2025, 3, Downloaded from https://advanced.onlinelibrary.wiley.com/doi/10.1002/admt.202400671 by Chung-Ang University, Wiley Online Library on [13/05/2026]. See the Terms and Conditions (https://onlinelibrary.wiley.com/terms-and-conditions) on Wiley Online Library for rules of use; OA articles are governed by the applicable Creative Commons License